Eur. Phys. J. B **21**, 205–210 (2001)

THE EUROPEAN PHYSICAL JOURNAL B

EDP Sciences

Pore size distribution in porous glass: fractal dimension obtained by calorimetry

R. Neffati and J. Rault[a]

Laboratoire de Physique des Solides, Université Paris-Sud, 91405 Orsay Cedex, France

Received 23 July 1999 and Received in final form 16 February 2001

Abstract. By differential Scanning Calorimetry (DSC), at low heating rate and using a technique of fractionation, we have measured the equilibrium DSC signal (heat flow) J_q^0 of two families of porous glass saturated with water. The shape of the DSC peak obtained by these techniques is dependent on the sizes distribution of the pores. For porous glass with large pore size distribution, obtained by sol-gel technology, we show that in the domain of ice melting, the heat flow J_q is related to the melting temperature depression of the solvent, $\Delta T_{\rm m}$, by the scaling law: $J_q^0 \sim \Delta T_{\rm m}^{-(1+D)}$. We suggest that the exponent D is of the order of the fractal dimension of the backbone of the pore network and we discuss the influence of the variation of the melting enthalpy with the temperature on the value of this exponent. Similar D values were obtained from small angle neutron scattering and electronic energy transfer measurements on similar porous glass. The proposed scaling law is explained if one assumes that the pore size distribution is self similar. In porous glass obtained from mesomorphic copolymers, the pore size distribution is very sharp and therefore this law is not observed. One concludes that DSC, at low heating rate ($q \leq 2$ °C/min) is the most rapid and less expensive method for determining the pore distribution and the fractal exponent of a porous material.

PACS. 81.05.Rm Porous materials; granular materials – 61.43.Hv Fractals; macroscopic aggregates (including diffusion-limited aggregates)

1 Introduction

The structural and dynamic properties of liquids trapped within the confined geometry of a porous solid have been the subject of considerable interest for many years. In all these porous materials the most studied liquid is water [1–4]. The effect of restricted geometry on the melting and freezing properties of cryogenic fluids [5], water [4,6], organic materials [6,7] and some metals [8–12] in porous glasses have been extensively studied by various experimental techniques: in particular calorimetry, acoustic technique, NMR and Wide angles X rays scattering (WAXS). In these materials filled with wetting (*e.g.* water) and non wetting (*e.g.* mercury) liquids one finds that the freezing and melting transitions are broadened and become hysteretic [4–12]. The broadening of the freezing thermograms in these materials, has been studied by different techniques: thermoporosimetry [4,6], gas desorption [13], Thermo Stimulated Current [14,15] (TSC) and NMR [13] and has been interpreted in term of the distribution of pore sizes. In most of the published works on porous materials a width of the pore size distribution is given but without giving a detailed analysis of the form of the distribution. Only a few authors have studied the fractal dimension of porous glass using various techniques but never by calorimetry.

Using small angle neutron scattering, with D_2O/H_2O water mixtures, Li *et al.* [16] demonstrated that the structure of Vycor glass can be visualised as a percolated network of pores, this network being somewhat reminiscent of Silica Aerogels, or branching polymers (both showing fractal geometry). It has been shown that below the peak at the scattering angle $\vartheta_{\rm m} = 0.025$ Å^{-1} observed by neutron scattering, the scattering intensity $I(\vartheta)$ follows the scaling law $I(\vartheta) \sim \vartheta^{-D}$, with the fractal volume dimension $D = 1.75$. In Silica sol-gel X-ray scattering at small angle [17] (SAXS) and NMR [18] studies lead to fractal dimension of the order of 2.2. Others porous systems have been studied and the fractal (volume) dimension lies between 2 and 3 [19].

Since the Thomson equation establish a direct relation between the temperature and the size scales, one can ask then if the melting thermograms of confined liquids in porous materials can give information on the pore size distribution, and eventually it's self similarity. The aim of this note is to compare by Differential Scanning Calorimetry (DSC) two different families of porous SiO_2 glass

[a] e-mail: rault@lps.u-psud.fr

(regular and irregular, with respectively narrow and large distribution of pore size) of similar mean pore size but of different size distribution. In the particular case of a self similar distribution (for porous glass from a sol-gel transition), one shows that the fractal dimension of the pore network can be deduced from the equilibrium DSC thermograms.

2 Materials

The first kind of material, called P123AC, is a SiO_2 glass templated by Pluronic triblock copolymers and using tetraethylorthosilicate as the silica source, the synthesis and morphology of this glass with cylindrical pores (in hexagonal array) has been given in references [21]. The diameter measured by Nitrogen Adsorption Desorption Isotherm is $d_{\mathrm{BJH}} = 4$ nm and by X-ray $d_{\mathrm{XR}} = 5$ nm and 7 nm (the d_{XR} value depending on the adopted model for the density profile between the pore and the matrix).

The second kind of materials is two Gelsil SiO_2 glasses (from Geltech) named G25 and G50. These materials have been obtained using sol-gel technology which gives a broad distribution of pore dimension. The mean pore size dimension of these two materials, given by Geltech, are respectively 2.5 and 5 nm, porosity 48 and 63% and internal surface areas [15], 610 and 580 m^2/g. These porous glass have been studied by several authors [15,22,24].

3 Experimental results

DSC measurements

In classical DSC, it is well known that the signal, the heat flow ($J_Q = \mathrm{d}H/\mathrm{d}t$) depends on the thermal conductivity of the sample, its mass m, the thermal contact sample - pan, and the heating and cooling rate $q = \mathrm{d}T/\mathrm{d}t$ [25]. These thermal effects explains the broadening of the enthalpy peak of pure compounds (ice) when the heating rate q increases. The important difference between bulk water and confined water is that the width of the melting of ice in porous glass does not extrapolates to zero for $q = 0$. This fact leads most of the authors [4–12] to interpret the observed width in different materials (polymer, porous glass) as being due to a distribution of crystallite sizes of the solvent. The major problem in calorimetric measurements, is the following: how slow must the heating rate be, in order to obtain a signal $J_Q^0/(m\,q)$ which is independent on the heating rate q, the mass of the sample and the thermal contacts.

The two kinds of porous glass have been saturated with water and analysed by a DSC Mettler instrument (DSC30). Typical heating thermograms, $J_Q(T)$, at low heating rate q for the two types of glass are given in Figures 1 and 2a. The mass of water absorbed in the porous glass is about 5 mg. The DSC instrument has been calibrated at $q = 0.5$ °C/min with pure water. One recall here that, for high heating rate, the temperature T_{m} corresponding to the maximum of the melting peak and the

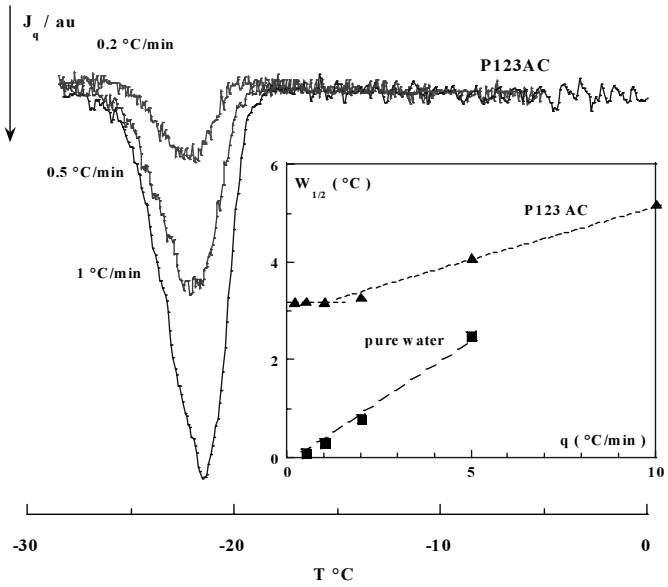

Fig. 1. Melting endhotherms of ice in P123AC porous glass: The heat flow J_Q *vs.* temperature heating rate $q = 0.2$, 0.5 and 2 °C/min. In the insert, width $W_{1/2}$ at half height of the melting peak of pure water and of water in these porous glass *versus* the scanning rate.

width of the melting peak increases with the amount of water in the DSC pan (typically the half width at half height is $W_{1/2} \sim 3$ °C for a mass of 8 mg). This is due to the finite thermal conductivity of the material and of the DSC pan.

Ordered P123AC porous glass

In the insert of Figure 1, we report the variation of the width $W_{1/2}$ at the half height of the melting peak of pure water and water in P123AC glass as function of the heating rate for the same mass (5 mg) of materials in the DSC pan. For $q \leq 2$ °C/min, one concludes that the width $W_{1/2}$ of the melting peak for the glass is not dependent on the heating rate. Similar experiments with different mass show that the width is also independent on the mass of water (for these heating rates). The pore size is given by the Thomson equation:

$$T_{\mathrm{m}} = T_{\mathrm{m}}^0 \left(1 - \frac{2\gamma_{\mathrm{sl}}}{\Delta H_{\mathrm{m}}^0} \nu \frac{1}{r}\right) \qquad (1)$$

where T_{m}^0 is the melting temperature of an ice crystal of infinite dimension, 273 K, γ_{sl} is the average interfacial tension of the crystal, $\gamma_{\mathrm{sl}} \sim 40 \times 10^{-3}$ N/m. $\Delta H_{\mathrm{m}}^0 = 334$ j/g is the specific melting heat. ν is the solid specific volume $\nu^{-1} = \rho = 0.971$ g/cm^3 and r is the crystal radius. The maximum of the DSC peak is situated at $T_{\mathrm{m}} = -22$ °C, which gives a mean pore diameter of 62 Å in good agreement with X-rays measurements.

The important point to remark, in Figure 1, is that for the three heating rates, $q = 0.2$, 0.5, 1 °C/min, the profiles of the thermograms are the same and can be fitted

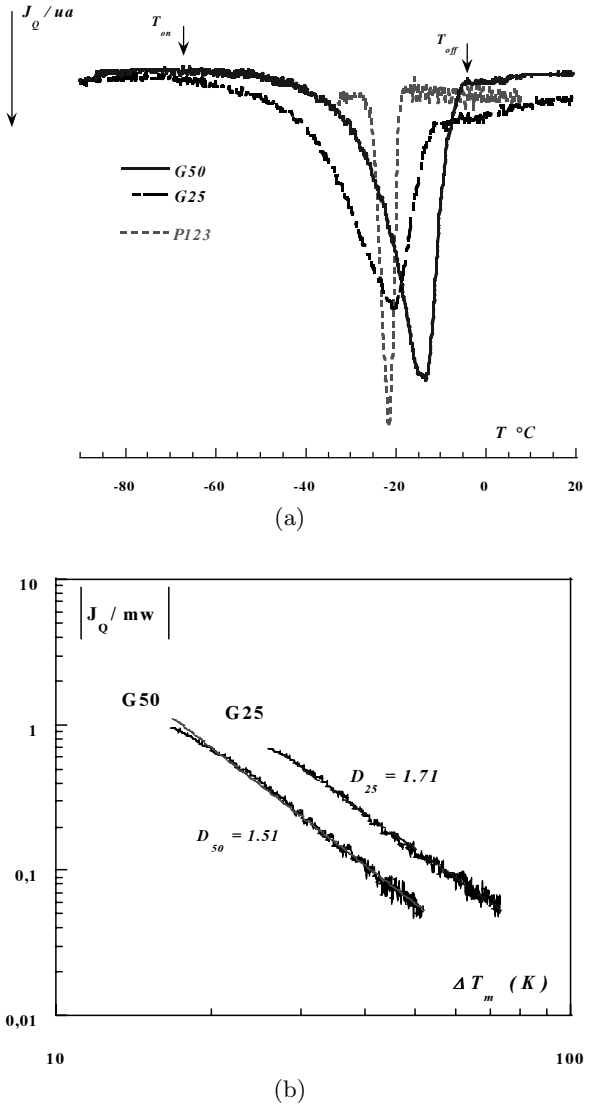

Fig. 2. Melting endhotherm of water in Gelsill glass, G25 and G50 and P123AC (for comparison). (a) Heat flow J_Q *vs.* temperature, heating rate $q = 2$ °C/min, $T_{\rm end}$ and $T_{\rm on}$ are the temperatures corresponding to the beginning and the end of the DSC peak for the G50 glass. (b) Heat flow J_Q *versus* the melting shift $\Delta T_{\rm m}$, on logarithmic scales.

by the same Gaussian curve $J_q \approx \exp -(T-22)^2/2\sigma^2$ with $\sigma = 0.7$ °C, the correlation factor is $\underline{R} = 0.98$, same fit is obtained for $q = 2$ °C/min. In such materials the width of the melting peak for $q < 2$ °C/min is an intrinsic parameter of the material and gives an indication of the distribution of the pore sizes.

From the DSC technique we conclude that the process of pore formation *via* the mesomorphic template leads to a very sharp Gaussian pore size distribution. Such a conclusion cannot be deduced from X-ray analysis because this last technique necessitates a model of the structure and because the SAXS spectra are widened by the disorientation of the glass grains which contain oriented cylindrical pores. These results show the great advantage of the calorimetric technique at low heating rate compared to SAXS. We have also demonstrated that calorimetry at heating rate higher than 2 °C/min (as usually done), gives wrong results concerning the mean pore dimension and the pore size distribution.

Disordered Gelsill porous glass

Classical DSC method. Typical DSC thermograms at $q = 2$ °C are given in Figure 2a; as the signal is broader (15 °C) than for the ordered porous glass (3 °C), the ratio signal/noise becomes too small at the lower heating rates and impedes the preceding analysis. The asymmetrical thermograms cannot be fitted by a Gaussian. In Figure 2b one shows that in a large domain of temperature (50 °C), between the beginning ($T_{\rm on}$) and the end ($T_{\rm end}$) of the melting, the heat flow has the scaling form, $J_Q \sim (\Delta T_{\rm m})^{D^*}$. Where $\Delta T_{\rm m} = T_{\rm m}^0 - T_{\rm m}$ is the shift of the melting temperature ($T_{\rm m}^0 = 273$ K). In these porous glass the melting is characterized by the temperatures $T_{\rm on}$, $T_{\rm end}$ and by the scaling exponents $D^* = 2.51$ and 2.71 (± 0.08) for samples G50 and G25 respectively, measured at the heating rate $q = 2$ °C/min. The paramount question is to verify these properties at lower heating rates. This is rather impossible with the classical DSC, because the signal to noise ratio become too small. It becomes then important to verify that the thermograms obtained at 2 °C/min is an equilibrium thermogram, as was the case for the preceding porous glass P123. This will be verified hereafter by the new DSC method called fractionated DSC described in reference [26].

Fractionated DSC.

To have thermodynamic thermograms of the melting of ice in porous glass (independent of the DSC drawbacks: scanning rate and delay times), the sample is submitted to thermal cycles involving 4 stages. The material is first crystallised during a DSC scan at 5 °C/min (stage 1). The total enthalpy of crystallisation is $\Delta H_{\rm c}$. Then the sample is reheated (stage 2) and annealed at temperature $T_{\rm a}$ in the melting region between $T_{\rm on}$ and $T_{\rm end}$ during a time $t_{\rm a}$ ($1'$, $5'$, $20'$) (stage 3). During a second cooling at 5 °C/min (stage 4) the thermogram is registrated. The subtraction with the base line gives the enthalpy of crystallisation $\Delta H_{\rm c}(T_{\rm a})$ of water which was previously obtained by the partial melting of ice at $T_{\rm a}$, during stage 2. This sequence is repeated for different temperatures of annealing.

By scanning the domain of melting by this method, one obtains a discrete thermogram $\Delta H_{\rm c}(T, t_{\rm a})$ which is an equilibrium thermograms if $\Delta H_{\rm c}$ is independent of the annealing time $t_{\rm a}$. The proportion in mass of crystallites which melt below T, during stage 2 and 3, is then $x(T) = \Delta H_{\rm c}(T)/\Delta H_{\rm c}^t$; $\Delta H_{\rm c}^t$ being the total enthalpy of crystallisation of the water measured during stage 1. In Figure 3a one reports this proportion for sample G25. Derivation gives the thermodynamical thermogram (at equilibrium) $J_Q^* \approx \dot{x}(T) \approx {\rm d}\Delta H/{\rm d}T$. We note that the

curves $x(T)$, for all the samples analysed, do not depend on the annealing time $t_a > 1'$. Therefore we state that $J_Q^* \approx \dot{x}(T)$ represents the true thermodynamic thermogram of water in Gelsill glass. In Figure 3b we compare the flow rates J_Q^* and J_Q of the G25 material as function of the supercooling ΔT in logarithm scales, obtained by the direct DSC method (at 2 and 10 °C/min) and by the fractionated DSC (curve F). The important point to note is that the classical DSC method at 2 °C/min gives thermograms very similar to that obtained by the fractionated method; the peaks of the thermograms are situated at the same temperature. The temperatures $T_{\rm end}$ are somewhat different, but in our opinion this is due to the lack of accuracy at the end of the ice melting. These two methods over a large domain of temperature (50 °C) below $T_{\rm m}(\sim -20$ °C) lead to the same scaling exponent $D^* = 2.7$. Most of the DSC thermograms published in the literature have been obtained at 10 and 20 °C/min and are therefore not true equilibrium thermograms; we conclude that by calorimetry with such high heating rate one cannot measure with accuracy the distribution of the pore distribution. The interest of the fractionated method is that the equivalent heat flow rate J_Q^* is much more important and accurate than the classical DSC flow rate J_Q, since it gives true temperatures (no delay times). In the stage 4 of this method, the cooling rate is arbitrarily 5 °C/min. The use of a more rapid cooling would increases the DSC signal but does not change conspicuously the form of the equilibrium thermogram. Higher cooling rates in stage 4 should be used for porous systems containing small amount of crystallizing solvent. The drawback of this new method is that for describing a thermogram containing n points, the time of experiment is of the $4nt$, t being the time of experiment by classical DSC (20′).

In conclusion, the above experiments on ordered and disordered porous glass shows that DSC measurements at heating rate $q = 2$ °C/min (or less) gives true information on the pore distribution of the porous structure (mean dimension and form of the distribution). Moreover the experimental method is relatively rapid (25 min per sample).

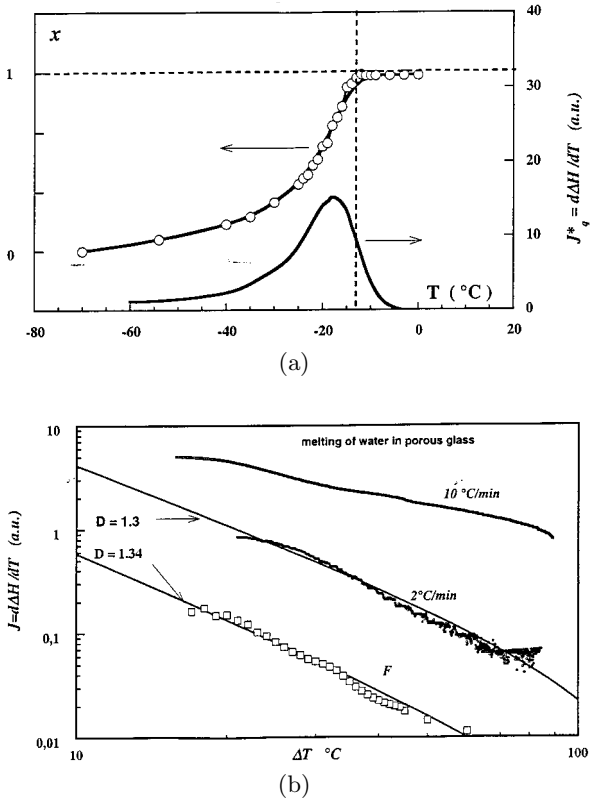

Fig. 3. (a) DSC fractionation of G25; proportion $x(T) = \Delta H_{\rm c}/\Delta H_{\rm c}^t$ of ice molten at annealing temperature $T_{\rm a} = T$; $\Delta H_{\rm c}$ is measured by the recrystallization procedure (stage 4 in the text). By derivation the equilibrium thermogram $J_Q^*(T)$ is obtained. (b) Comparison between classical DSC at 10 and 2 °C/min and the fractionated DSC method (curve F). Heat flow *versus* supercooling ΔT on logarithmic scales. For more clarity the curves are shifted arbitrarily vertically. The fractal exponents D deduced from the slopes of the two curves F and 2 °C/min are found to be nearly equal. The lines are the fits from equation (6) (see Tab. 1) assuming that the melting enthalpy is given by equation (3b) with $T_{\rm K} = -120$ °C.

4 The origin of the scaling law

The Thomson equation (Eq. (1)) can be put in the simple form:

$$t_m = \frac{a_T}{r} \tag{2}$$

where $(T_{\rm m}^0 - T_{\rm m})/T_{\rm m}^0$ is the reduced melting temperature and $a_{\rm T} = \frac{2\gamma_{\rm sl}}{\Delta H_{\rm m}}\nu$ is a length called the Thomson length. Typically $a_T = 2.5$ Å for water. In most of the published works the melting enthalpy $\Delta H_{\rm m}$ is temperature independent. Brun [6] has shown that the crystallizing enthalpy $\Delta H_{\rm c}$ of water in porous silica and alumina decreases with the freezing temperature $T_{\rm c}$, according to the experimental relation:

$$\Delta H_{\rm c}(T_{\rm c}) = 332 - 7.43\Delta T_{\rm c} + 5.56(\Delta T_{\rm c})^2. \tag{3a}$$

In the domain 25 K $< \Delta T_{\rm c} = 273 - T_{\rm c} < 0$ K the variation are linear $\mathrm{d}\Delta H_{\rm c}/\mathrm{d}T \sim 6$ J/g K, and there is no reason to postulate that the variations of $\Delta H_{\rm c}(T_{\rm c})$ and $\Delta H_{\rm m}(T_{\rm m})$ are different.

When the melting depression temperature becomes important $(T_{\rm m}^0 - T_{\rm m}) > 10$ °C, Hofmann [27] and Gelb *et al.* [28] have proposed that $\Delta H_{\rm m}$ varies linearly with the temperature. In fact one can postulate that the melting enthalpy is given by the following linear relation:

$$\Delta H(T_{\rm m}) = \Delta H_{\rm m}^0 \left(\frac{T_{\rm m} - T_{\rm K}}{T_{\rm m}^0 - T_{\rm K}}\right) = \Delta H_{\rm m}^0 \left(1 - \frac{t_{\rm m}}{t_{\rm K}}\right) \tag{3b}$$

where $T_{\rm K}$ is the Kauzmann temperature [29], a characteristic temperature of the liquid of the order $T_{\rm m}^0/2$. In most of the glass forming materials $T_{\rm K}$ coincides with the T_0 temperature where the relaxation time extrapolates to infinite. It must be recalled here that the differences in

specific volume and in enthalpy between the crystal and the liquid phases decrease linearly when the temperature decreases, and extrapolates to zero at T_K. For water the temperature T_K is not known accurately, but this will have no influence on ours conclusions.

To explain the value of the fractal dimension one assumes that the pore size distribution $P(r)$ follows, under a certain size, the power law:

$$P(r) = \frac{dx}{dr} \sim r^{D-1} \tag{4a}$$

where dx is the fraction of crystallite having size between r and $r + dr$ and which melt between T_m and $T_m + dT_m$. This assumption is suggested by the fractal character of these porous systems obtained by sol-gel transition. The total volume of pore $V(r)$ obtained by integration is then given by the classical law

$$V(r) \sim r^D \tag{4b}$$

where D is the fractal dimension of the structure.

As the fraction dx of crystallites melting between T_m and $T_m + dT_m$ is $J_Q dT_m/\Delta H(T_m)$, one has the relation:

$$\frac{dx}{dT_m} = \frac{dx}{dr}\frac{dr}{dT_m} = \frac{J_Q^*}{\Delta H_m(T_m)}\,. \tag{5}$$

Then using the Thomson law (2) and the distribution law (4), one obtains the relation between the heat flow $J_Q^* = (J_Q)_{q\to 0}$ extrapolated at zero heating rate and the melting temperature shift ΔT_m:

$$(J_Q^*) \sim (\Delta t_m)^{-(D+1)} \Delta H_m(T_m). \tag{6}$$

Assuming that the melting (or crystallization) enthalpy is constant, from the Figure 3b we deduce that the fractal exponents are $D = 1.7 \mp 0.1$ and $D = 1.5 \mp 0.1$ respectively for the two Gelsill glasses G25 and G50 in a range of temperature of 50 °C between the beginning of melting T_{on} and the end of melting T_{end}. This must be compared to the fractal dimension, $D = 1.75$, measured by Li *et al.* [16] on similar glass (Vycor) by small angle neutron scattering, in the scattering range $0.003 < q < 0.02$ Å^{-1}. By both techniques, in the domain of application of the power law, the signal (neutron scattering intensity and DSC heat flow) varies over 1.5 decades. By electronic energy transfer (EET), Even *et al.* [30] and Arndt *et al.* [23] measured the same fractal dimension (in volume), which is considerably smaller than the value 2.5 for a percolation cluster in three dimensions and close to the backbone fractal dimension $d_B = 1.855 \pm 0.015$ [19]. the three dimensional cluster backbone is obtained by erasing the dangling branches from the percolation cluster [20].

In fact the exponent is very sensitive to the exact form of the temperature variations of the melting enthalpy. In the following table we give the value of the exponent $D+1$ for the G50 sample when $\Delta H(T_m)$ is assumed to be given by equations (3a, b) or is constant. For these three fits the correlation factor $\underline{R}$ of the fit has the same value 0.997. From this we conclude that the Brun and Kauzmann relations leads to very different D values. Recently it has been shown that the melting enthalpy of several liquids present linear variations with T as expected from the Kauzmann relation [31]. Therefore the exact value of the fractal exponent of the porous structure, *via* our method, necessitates a precise knowledge of the Kauzmann temperature. This is not the case for water which has a very complex behavior in the supercooled state [1–4].

Melting enthalpy $\Delta H_m(T_m)$	$D+1$	$\underline{R}$
ΔH_m = const.	2.5	0.997
Kauzmann variation Eq. (3b)		
$T_K = -120$ °C	2.2	0.997
$T_K = -60$ °C	2.34	0.997
Brun variation Eq. (3a)	1.7	0.998

5 Conclusion

The DSC thermograms obtained at low heating rate ($q <$ 2 °C/min) and by the fractionated method are characteristic of the fractal nature of the pore network of the different porous glass. In ordered porous glass like P123 AC, obtained from the mesomorphous phase of copolymers, the distribution of the pore size is very sharp, until now the porometry method is the only method which gives an estimate of the fluctuation of the pore diameter (±0.5 nm). In porous glass like Gelsill obtained by sol-gel techniques, the thermograms are very large. This in principle impedes drawing off firm conclusions from the classical DSC at low heating rate. Using the DSC fractionated method we have shown that the equilibrium melting curve and the melting curve obtained by the classical DSC at 2 °C/min are very similar. From these two types of ice melting curves, we measure a fractal exponent D^*, which can be related to the exponent D of the power law given the pore size distribution (Eq. (4)). The exponent, $D = D^* - 1$, is found to be dependent on the temperature variation of the melting enthalpy. If one assumes that $\Delta H(T_m)$ follows the Kauzmann relation (Eq. (3b)) then we find an exponent D of the order 1.3 which is comparable with the fractal exponent, 1.7, obtained by others techniques on similar porous glass obtained by spinodal decomposition. The fractal exponent D^* is an intrinsic parameter of porous glass and it would interesting to compare the D^* values of different porous materials. It may also be important in the future to relate the cross-over temperatures T_{on} and T_{end} to mean dimensions of the fractal structure of the material. Finally we stress that DSC came out at a heating rate (2 °C/min) is the most rapid and inexpensive method for determining the pore size distribution and the fractal exponent of a porous material. In our opinion, it is also the most accurate technique (see for comparison Fig. 2 of reference [13], giving the pore size distribution of similar silica obtained by NMR).

The authors thank L. Apekis and A. Davidson for providing the Gelsill and P123AC glass and for fruitful discussions. Also we want to thank R. Botet for fruitful discussions.

References

1. D.C. Steyler, J.C. Dore, J. Chem. Phys. **87**, 2458 (1983).
2. L. Bosio, G.P. Johari, M. Oumezzine, J. Teixeira, Chem. Phys. Lett. **188**, 113 (1992).
3. M.C. Bellissent-Funel, J. Lai, L. Bosio, J. Chem. Phys. **98**, 4246 (1993); M.C. Bellissent-Funel, K. Bradley, S.H. Chen, J. Lai, Physica A **201**, 277 (1993).
4. Y.P. Handa, M. Zakrzewski, C. Fairbridge, J. Phys. Chem. **96**, 8594 (1992).
5. E. Moltz, A.R. Wong, M.H. Chan, J.R. Beamish, Phys. Rev. B **48**, 5741 (1993).
6. M. Brun, Ph. D. thesis, University of Lyon, France, 1973; M. Brun, A. Lallemand, J.F. Quinson, C. Eyraud, Thermochim. Acta **21**, 59 (1977); J.F. Quinson, M. Brun, in *Characterization of Porous Solids*, edited by K.K. Unger, J. Rouquerol, K.S.W. Sing (Elsevier, Amsterdam, 1988), p. 307.
7. C.L. Jackson, G.B. McKenna, J. Chem. Phys. **93**, 9002 (1990).
8. K.M. Unruh, T.E. Huber, C.A. Huber, Phys. Rev. B **48**, 9021 (1993).
9. B.F. Borisov, E.V. Charnaya, Y.A. Kumserov, A.K. Radzhabov, A.V. Shelyapin, Solid State Commun. **92**, 531 (1994); E.V. Charnaya, C. Tien, K.J. Lin, Y.A. Kumserov, Phys. Rev. B **58**, 11089 (1998).
10. Y.A. Kumzerov, A. Naberezmov, S.B. Vakhrushev, B.N. Sovenko, Phys. Rev. B **52**, 4772 (1995).
11. B.F. Borisov, E.V. Charnaya, P.G. Plotnikov, W.-D. Hoffmann, D. Michel, Y. Kumzerov, C. Tien, C.-S. Wur, Phys. Rev. B **58**, 5329 (1998).
12. E.V. Charnaya, C. Tien, K.J. Lin, Y. Kumzerov, Phys. Rev. B **58**, 11089 (1998).
13. J.H. Strange, M. Rahman, E.G. Smith, Phys. Rev. Lett. **71**, 3589 (1993).
14. R. Pelster, A. Kops, G. Nimtz, A. Endos, H. Kietzman, P. Pissis, A. Kryritsis, S. Woerman, J. Phys. Chem. **667**, 1003 (1997).
15. P. Pissis, J. Laudat, A. Kyritsis, J. Non-Cryst. Solids **171**, 201 (1994); P. Pissis, D. Daoukaki-Diamanti, L. Apekis, J. Phys. Cond. Matt. **6**, L325 (1994); P. Pissis, A. Kyritsis, D. Daoukaki, G. Barut, R. Pelster, G. Nimitz, J. Phys. Cond. Matt. **10**, 6205 (1998).
16. J.C. Li, D.K. Ross, J. Phys. Cond. Matt. **6**, 351 (1994); J.C. Li, D.K. Ross, R.K. Heeman, Phys. Rev. B **48**, 6716 (1993).
17. D.W. Schaefer, K.D. Keefer, Phys. Rev. Lett., **56**, 2199 (1986).
18. F. Deveux, J.P. Boilot, F. Chaput, B. Sapoval, Phys. Rev. Lett. **65**, 614 (1990).
19. D. Avnir, D. Farin, P. Pfeiffer, Nature **308**, 261 (1984).
20. A. Bunde, S. Havlin, *Fractals and Disordered Systems* (Springer, New-York, 1995).
21. Y. Bennadja, P. Beaunier, D. Margolese, A. Davidson, Microporous Mesoporous Mater. (in press); M. Imperor-Clerc, P. Davidson, A. Davidson, J. Am. Chem. Soc. **123**, 11925 (2000).
22. C. Streck, Y. Mel'Nichenko, R. Richert, Phys. Rev. B **53**, 5341 (1996).
23. M. Arndt, F. Kremer, Mater. Res. Soc. Symp. Proc. **366**, 259 (1995).
24. W. Gorbtschow M. Arndt, R. Stannarius, F. Kremer, Europhys. Lett. **35**, 719 (1996).
25. V. Bershtein, V. Igorov, *Differential Scanning Calorimetry of polymer: Physics, Chemistry, Analysis, Technology* (Ellis Horwood, NY 1994).
26. R. Neffati, L. Appekis, J. Rault, J. Thermal Analysis **54**, 741 (1998).
27. J.D. Hofmann, J. Chem. Phys. **28**, 1192 (1958).
28. L.D. Gelb, K.E. Gubbins, R. Radhakrishnan, M. Sliwinska-Bartkowiok, Reports Prog. Phys. **62**, 1573 (1999).
29. A.W. Kauzmann, Chem. Rev. **43**, 219 (1948).
30. U. Even, K. Rademann, J. Jortner, N. Manor, R. Reisfeld, Phys. Rev. Lett. **52**, 2164 (1984).
31. R. Neffati, Ph.D. thesis, Université de Paris-Sud, Orsay, 1999.